Transient Heat Flux Assessment Using a Platinum Thin Film Sensor for Short-Duration Applications

Sumedh Dongare
Visvesvaraya National Institute of Technology
Ravi K. Peetala
ravipeetala@nitw.ac.in

National Institute of Technology Warangal
Trushar B. Gohil
Visvesvaraya National Institute of Technology
Nidhish Agrawal
Visvesvaraya National Institute of Technology
Akash Jadhav
Visvesvaraya National Institute of Technology

Research Article

Keywords: TFGs, Sensitivity, TCR, Calibration, Heat flux measurement

Posted Date: December 14th, 2023

DOI: https://doi.org/10.21203/rs.3.rs-3725840/v1

Additional Declarations: No competing interests reported.

Version of Record: A version of this preprint was published at Heat and Mass Transfer on April 8th, 2024.
See the published version at https://doi.org/10.1007/s00231-024-03473-0.

“Transient Heat Flux Assessment Using a Platinum Thin Film Sensor for Short-Duration Applications"

Sumedh Dongare[#], Ravi K. Peetala*, Trushar B. Gohil[#], Nidhish Agrawal[#], Akash Jadhav[#].

#Department of Mechanical Engineering, Visvesvaraya National Institute of Technology, Nagpur, 440010, India

*Department of Mechanical Engineering, National Institute of Technology, Warangal, 506004, India

Manuscript Submitted to the Journal

Heat and Mass Transfer

Correspondence:
Dr. Ravi K. Peetala
Associate Professor
Department of Mechanical Engineering
National Institute of Technology, Warangal
Warangal – 506004, India
Email: rkpeetala@mec.vnit.ac.in
Phone: +91 98848 89299

December 2023

“Transient Heat Flux Assessment Using a Platinum Thin Film Sensor for Short-Duration Applications"

Abstract:

The rapid fluctuations in heat transfer rates make it challenging to determine the surface temperature history and the estimation of accurate heat generation in research applications such as IC engines, gas turbines, and high-speed space vehicles. Therefore, thin-film gauges (TFGs) are generally used to measure the heat flux in such applications due to their high sensitivity and quick response time. The present study demonstrates that increasing the annealing heat treatment temperature, will enhance the adhesion of the thin film and the capabilities of these hand-made thin-film gauges for transient measurements at low temperatures and for short periods. In the present work, TFG is fabricated in-house using platinum as a sensing element and Macor as an insulating substrate. The sensitivity (S) and temperature coefficient of resistance (TCR) are estimated using an oil batch calibration technique. At the same time, the performance of TFG is tested in a dynamic convective environment. The TFG is exposed to the convective environment using a designed calibration set-up, and their transient heat fluxes are computed by conducting several trials. Additionally, the numerical solution has been accomplished using various experimental parameters. In comparison to the outcomes of the experimental method, it is observed that the average fluctuating temperature and mean surface heat flux have an inaccuracy of 0.33% and 4.17% respectively.

Keywords: *TFGs, Sensitivity, TCR, Calibration, Heat flux measurement.*

Nomenclature

R	electrical resistance (Ω)
R_a	average roughness (μm)
R_h	resistance during heating (Ω)
R_c	resistance during cooling (Ω)
k	thermal conductivity (W/mK)
C	specific heat (J/kg-K)
$\sqrt{\rho Ck}$	thermal effusivity (J/m^2 s$^{0.5}$ K)
T	temperature (K or °C)
S	sensitivity (ohm/K)
r	coefficient of correlation
t	test time (s)
I	current supplied (A)
q	heat flux (W/m^2)

Abbreviations

TFGs	Thin film gauges
TCR	Temperature coefficient of resistance
CCS	Constant current source
DAS	Data acquisition system
RTD	Resistance temperature detector
MWCNTs	Multi-walled carbon nanotubes
TFHFS	Thin film heat flux sensors
PTFHFS	Platinum thin film heat flux sensors
SEM	Scanning electron microscope

Greek letters

ρ	density (kg/m^3)
β	angle with X-axis (^{o})
ᾳ	thermal diffusivity (m^2/s)
γ	temperature coefficient of resistance (K^{-1})
Δ	difference

Subscripts

s	Substrate
0	room temperature
h	heating
c	cooling

1. Introduction:

In engineering applications that involve heat, different types of reactions, and physical interaction occurring in a heated environment near surfaces or walls, it is important to have a thorough understanding of the temperature changes on the wall surfaces and the rate at which they are being heated. This knowledge is vital for the efficient design of various systems such as gas turbines, aerodynamic vehicles, cooling devices, boilers for low-speed flows, and other related technologies. Measuring heat transfer is essential because heat transfer conditions are changing rapidly, in each of these cases, the dominant physical quantity in motion is the heat flux, which represents the flow of thermal energy through a surface. For short-duration heat flux measurement applications, the adhesion of thin film gauges plays an important role because it improves temperature and heat flux data acquisition accuracy and reliability, which is critical for a variety of applications such as automotive, aerospace, and industrial areas. The thin film gauges that have been designed facilitate direct application on heated surfaces of any shape, which is crucial for accurately measuring applications that have rapidly fluctuating surface temperatures [1]. These measurements are then used as inputs to obtain the local heat transfer rates using an appropriate numerical approach. On the other hand, estimating the surface heat flux has been an inverse problem that demands temperature measurement. Furthermore, because of the frequent temperature variations or short experiment periods, heat flux estimation becomes extremely crucial. Low-response-time thermal sensors continue to be necessary due to this strict requirement. Thin film heat flux sensor (TFHFS) typically uses paints that respond to temperature, calorimeter indicators, and co-axial thermocouples to measure heat flux following temperature. Since TFHFS have a very quick response time and are useful for various applications, they are typically preferred. In 1956, Vidal invented this sensor to measure the rapid heat transfer inside a shock tube.

The literature suggests that numerous forms of TFHFS have been introduced. Several TFHFS are prepared by depositing a conducting layer (silver, nickel, or platinum) on a substrate with insulation (Macor, quartz, or Pyrex). Sputtering or spraying sensing film affixed onto a backing material is one of those processes in the sensor-making process, but it is an essential component of that process. Because it impacts how well heat conducts through solids, the backing material's surface roughness remains a key factor in this phase. It has also been investigated how surface roughness affects thin films' resistivity [3–7]. *Krzak-Ros et. al.* performed investigations to determine how surface roughness affects the compositions of TiO_2 and SiO_2 [8]. If the substrate roughness is greater than 2.5 μm, researchers noticed the typical breaking in the film. Rough Substrate is another factor that might influence interfacial adhesion. To relate the impact of surface roughness upon adhesion, theoretical and numerical approaches have been created and studied [9–11]. In certain research, a thin layer was painted on enamel-coated metal samples to evaluate heat transfer [12]. The use of a flexible plastic sheet with an instrumented, sputtered thin film was also reported in some research studies [13]. The sensor's ability to quickly detect changes in temperature fluctuations caused by thermoacoustic instability is enhanced by its high sensitivity and low response time [14]. Usually, these sensors are used to estimate how much heat will pass through turbine blades as well as rotors. Due to their simplicity in construction, quick response times, measurement accuracy, and flexibility to test models of various forms, TFHFS has been selected as the preferred method of measurement for heat transfer in different facilities, including shock tunnels, shock tubes, and expansion tubes. This could include experiments involving thin-walled hollow models, longer test durations, or intensive investigations of three-dimensional conduction involving the potential utilisation of double-sided gauges [15-16]. A conductive thin film made of materials like platinum, nickel, or silver is usually observed on insulating substrates such as Pyrex, Macor, or

quartz. The parameters will determine the dimensions, and the shape of the substrate is not a critical factor; however, the substrate must have sufficient depth to uphold the assumption that it is a semi-infinite solid. In some circumstances, it can be challenging to fulfill the requirements of a semi-infinite solid. To determine the time-dependent surface heat flux, various analytical techniques were used to deal with the heat conduction problems of a semi-infinite body [17-18].

Although this gauge is ideal for measuring temperature gradients across insulating layers, its production can be quite intricate. There are various techniques for producing thin films, including vacuum coating, sputtering, and hand painting using specialised brushes and the TFGs were fabricated at 600–650 ℃ heat treatment temperature range. The thickness of thin films is often limited to a few micrometers. The TFHFS works on the same principles as a traditional resistance temperature detector (RTD), in which a connection to a steady current source (CCS) is needed. Here, it is predicted that the electrical resistance of TFHFS will change linearly with temperature. However, calibration of each TFHFS individually is necessary before installation to analyse the variation of response voltage to temperature and determine the slope to ensure linear behavior. However, each TFHFS must be individually calibrated before being used for an actual measurement. There are two calibration methods, called static and dynamic calibration methods that can be found in the literature. The sensitivity and TCR are two parameters that are typically measured using the static calibration method. However, using dynamic calibration, when TFHFS are exposed to a given heat load, it is possible to measure their thermal performance. The three types of heat transfer that can be used to apply such heat loads. *Kumar et. al.* [19–22] The TFHFS on a Pyrex substrate has been fabricated by annealing heat treatment at 650 ℃, and radiative and conductive modes have been used to calibrate them. In certain experiments, it was found that the heat flux recovery had very little variance, approximately 2%. *Sahoo et. al.* [23–24] The TFGs were exposed gradually at a temperature of 650 °C, then performed static calibration using oil-based procedures and dynamic calibration of coaxial thermocouples using radiation and conduction modes of heat transfer. Which are nearly equivalent to the heating environment encountered by an aerodynamic model in short-duration impulse facilities. *Jadhav et. al.* [25] The TFGs are annealed to 650°C and selected for conduction-based calibration for their TFHFS improvement. *Sahoo et. al.* [26] Examined the transient response characteristics and evaluated the performance of a calorimetric surface junction probe under impulsive thermal loading was undertaken. *Goswami et. al.* [27] by using a blast furnace to dry the film at a temperature of about 650 ℃ and dynamically calibrated temperature sensors based on light rays is used for measuring transient changes in temperature. *Nguyen et. al.* [28] demonstrate the capability of a new active thermal microchip specialized for temperature calibration of scanning thermal microscopy (SThM) probes and reveal that a smaller region of the temperature sensor will be necessary to evaluate the disturbance in the local area of contact. *Sarma et. al.* [29] employed convective heat transfer techniques to measure the silver TFHFS. The results indicated that platinum TFHFS are more reliable than silver TFHFS due to the latter's tendency to deviate from linearity. *Tiggelaar et al.* [30] examine Pt/Ta thin films have much higher electrical characteristics and adhesion than Pt/Ti films above 650 ℃. *Hamdi, M. et al.* [31] The annealing temperature significantly influenced the Adhesion of the coatings.

Additionally, *Smith et al.* presented a comparison of convection and radiation modes. Consequently, a calibration of TFHFS is always necessary to evaluate their performance metrics, such as TCR and Sensitivity. By using calibration constants derived from the recorded temperature signals, it is possible to reconstruct past data on local surface heat flux. *Sangbeom et. al.* [32] Characterize the heat transfer performance of a vapour chamber coupled

into a microelectronic packaging substrate. *Alam et. al.* [33] examines how the TFHFS are appropriate for conducting short-term assessments based on conduction. TFHFS output would be obtained during the actual experiment for measuring heat transfer, and this output combined with an appropriate heat conduction modelling approach helps calculate a surface heat flux. TFHFS are activated in these experiments using a steady-current supply. These sensors change their resistance when subjected to heat loads, allowing for the recording of voltage signals. The voltage variation is converted into a temperature signal using the known TCR value calculated from calibration trials. Consequently, to make surface heat transfer measurements, one can first measure the recorded surface temperature history, which can be utilised along with the appropriate analytical technique, such as one-dimensional heat transfer in a semi-infinite solid, to analyze the collected data. These inverse heat conduction problems can be solved using several numerical techniques that are described in the available literature. *Cook et. al.* developed a heat flow recovery algorithm based on a linear spline fit from the experimentally recorded voltage signal. Different kinds of analytical techniques were utilized to address the heat conduction challenges associated with a semi-infinite solid, to determine the time-dependent surface heat flux along this dimension [34–35]. *Sahoo et al.* used several methods, such as cubic spline, polynomial fitting, and piecewise linear fitting, to discretize the temperature signals and predict the inverse heat flux [36–38].

In many instances, TFGs have been fabricated through annealing at 650 °C. However, in many studies, it has been observed that adhesion at this temperature is inadequate. The present work aims to address this issue through experimental analysis. The annealing heat treatment temperature of 900 °C is used in the present work. The experimental findings revealed improved adhesion of thin film at this temperature, as verified through visual inspection. Rubbing the sensor's deposited film on 1000-grit-size sandpaper and experiment by exposing it in a convective-based environment. However, the adhesion is not quantified in the present study. In this work, a platinum thin-film gauge is fabricated and calibrated in a lab. To determine the TCR and sensitivity, a static calibration technique is adopted. Calibration, in this context, involves the process of assessing and fine-tuning the precision and accuracy of handcrafted thin film gauges. It is very crucial to justify the applicability of TFG and its effectiveness in convection applications by calibrating it in similar environments. In this regard, transient heat flux measurement was conducted in a low-temperature and low-velocity forced convective environment using a commercially available hot air gun. The fabricated TFG is exposed to two distinct and known combinations of input velocity and temperature using the simple laboratory experimental setup. The TFG is subjected to convective flow using a hot air gun for brief intervals of 1 second. Subsequently, the transient temperature variations over time during the period of exposure are recorded using a data acquisition system (DAS). For the same experimentation circumstances, Numerical simulations are carried out employing commercially available software (ANSYS-FLUENT). The transient surface heat fluxes are recovered by employing a one-dimensional heat conduction model designed for a semi-infinite object. This estimation is based on the transient temperature data obtained from the platinum-based TFG through experimental measurements and numerical simulations. This manually crafted TFG is capable of measuring the heat flux under conditions of low velocity and temperature.

2. Thin Film Gauge Fabrication in-house

2.1 Preparation of the substrate

TFGs are made using a substrate and a Macor rod of 6 mm in diameter and 10 mm in depth. Using silicon carbide sandpapers (3M, India) of various grits 600, 1200, and 2000, the Macor rod has been polished. Adequate care has been taken during this polishing operation to maintain the surface smooth. The Macor rod is cleaned with ethanol

and then washed with distilled water before the substrate roughness is measured. These rods are subsequently cleaned in an ultrasonic solution to remove adherent dust particles and maintain an impurity-free surface. The desired surface was scanned along its four paths using a commercially accessible surface roughness analyzer (Mitutoyo, Japan; Model-SJ-410), as illustrated in Fig. 1. An average surface roughness (Ra) is tested to quantify the roughness. Ra essentially stands for an arithmetic mean of the irregularities in roughness Calculated by determining the mean value of the line that passes through the sampling length. Here, the angle β is determined by measuring it for the X-axis anticlockwise, with 45° increments between 0° and 180° as shown in Fig.2. As a result, the sample roughness graph obtained is shown in Fig. 1. Along the four directions, the average variation (from the average value) is 4.23% for the sandpaper of a 2000 grit size, respectively. This allowed range of 5% variances substantially indicates that the current substrate preparation method yields a surface with a fairly consistent roughness.

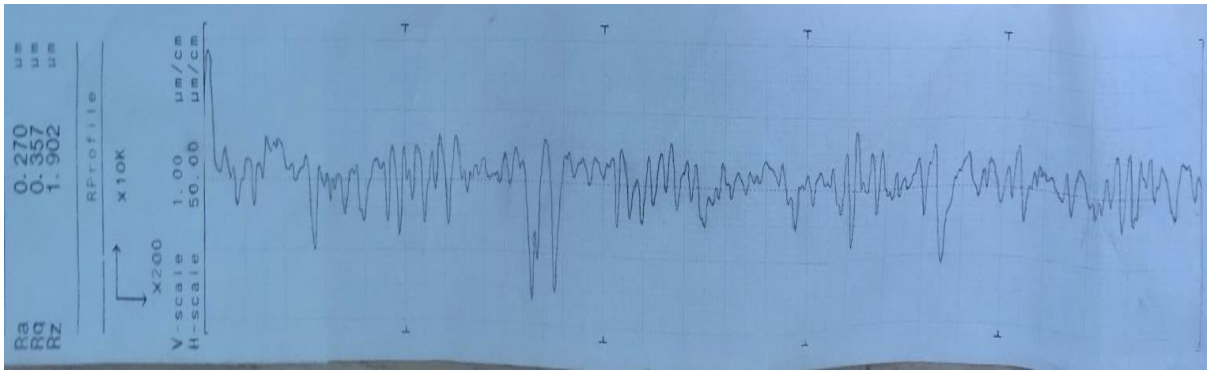

Fig.1: The roughness profiles of the substrate samples treated with sandpaper having a grit size of 2000 are shown.

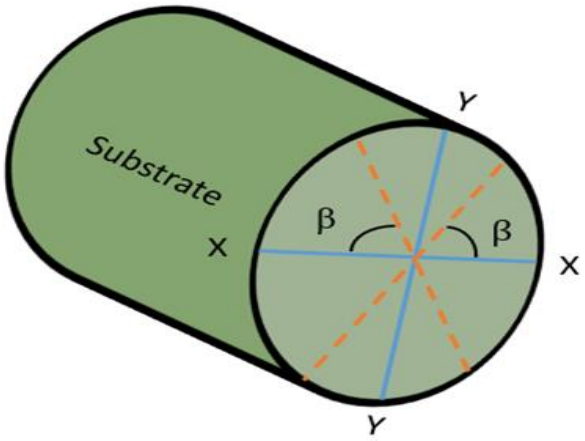

Fig. 2: Measurement of the roughness along the four trajectories at a 45° angle

2.2 Preparation of backing material:

The TFGs consist of three primary components: the substrate and thin films for sensing and connecting, as illustrated in the Fig.3 This study uses platinum as the sensing material because of its inertness and uniform TCR over a wide temperature range, making it the preferred material for TFGs or RTD thin film fabrication [9]. Macor is the type of ceramic utilized as the substrate material (RS component, India). Due to its poor thermal conductivity, Macor is the perfect substrate material. Good insulating qualities are needed. To verify the accuracy of the assumption that the slab is semi-infinite, Macor can be heated up to 1000 °C without undergoing any

noticeable geometric distortion. During gauge preparation, temperatures approaching this value are necessary. It should be affirmed that this material is simple to machine, enabling it to connect gauges to complex geometrical structures. Although Macor exists in a variety of geometries, developing rapid-response RTDs for temporary facilities is feasible and practical with a tiny cylindrical substrate [40]. This experiment employed solid cylindrical rods that were approximately 10 mm in length and had a diameter of 6 mm. The thin silver film connects electrical systems between the connecting wires and the sensing thin film. Table 1 provides information on the thermophysical characteristics of the substrate and sensing components at 27 °C ambient temperature. The substrate is polished as the first stage in the development of TFGs to ensure that the surface to be painted with the film is smooth. In this scenario, polishing is performed using sandpapers of three different grit sizes of metallurgical grade. The substrate is initially polished with sandpaper of 600 grit size, and smoothing is then carried out using 1200 and 2000 grit size sandpaper for about the same period. The edges are then polished and chamfered utilizing the same papers that prevent film breakage owing to their sharpness. After finishing, the substrates are subjected to ultrasonic washing for 20 minutes and washed with an ethanol cleaning solution. Because contaminants may affect the sensor's responsiveness, this process is crucial to ensure the cleanliness of the substrate's surface [38]. The substrates are then dried for 15 minutes at 60 to 70 °C under a heating light.

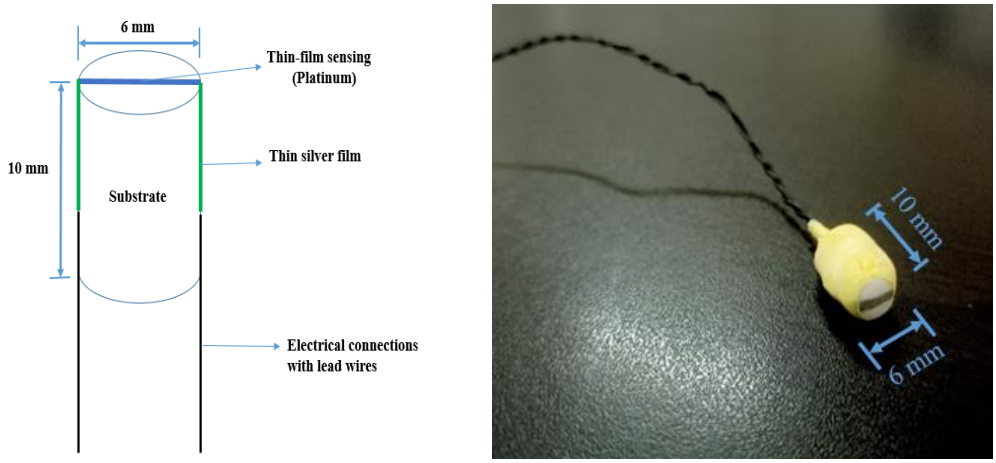

(a) (b)

Fig. 3: Heat flux sensor built with thin film (a) schematic (b) actual photograph

2.3 Developing pure platinum TFG

Commercially available metallo-organic paint preparations with 99.99% purity are used to create the pure platinum TFGs (SPI Supplies, USA). The thin layer is deposited on the substrate using a specialized brush (Camlin, India) with fine hairs. The sensitivity of the sensor is affected by the films' length-to-width ratio [42]. The studies maintain this ratio at 2.5. Following this procedure, all substrates are dried for 20 minutes under a high-powered heating lamp to remove all chemical agents and ensure the film is fully dried. The substrates coated with paint are annealed in a muffle furnace powered by a microcontroller to reduce thermal stresses as well as stabilise the calibration variables (TCR and sensitivity). To prevent cracks from forming, the temperature gradually increases to 900 °C over two hours with a constant heating rate.

Table 1: Materials' temperature-dependent properties [22, 40]

Material	k (W/mK)	c (J/kg-K)	ρ (kg/m^3)	$\sqrt{\rho ck}$ (J/m^{2}s$^{0.5}$K)
Macor	1.46	790	2520	1704.86
Platinum	70	130	21,500	13,987.50

The electrical connections are then made using silver metallo-organic paint (obtained from SPI Supplies, USA).On the substrate, two silver thin films are deposited opposite one another. This thin film is intentionally created very thick and retained at half the thickness of the substrate (5 mm) to maintain a low resistance in comparison to the resistance of the platinum thin film. The platinum thin film is carefully extended onto the side surfaces of the backing material to minimize the overlap between the platinum and silver thin films. As a result, the sensing surface would not exhibit a silver film. Silver and platinum both serve as detecting elements in sensors where the overlap on the sensing surface is greater than what is required. Along with increasing the resistance of the effective film, it would also cause nonlinearity to be noticeable in static calibration [26]. After 30 minutes of annealing at 350 °C in a muffle furnace, those painted substrates can naturally cool to ambient temperature. Electrical connections are made using insulated copper wires that are 2 meters long and 0.4 mm in diameter. The thin silver films were soldered against the wires with sufficient caution and then Teflon tapes were used to strengthen the design. Fig. 3. depicts such a fabricated sensor.

2.4. Basic Characterisation of Thin Film:

XRD analysis:

X-ray diffraction (XRD) tests were performed on a special material known as Macor using a D/tex Ultra 250 advance diffractometer (Smart Lab, Rigaku) with the Cu-Kα (λ= 0.15406 nm) radiation in the operating range of 2θ values of 20° to 100°, scan rate of 2º per min., and step size of 0.02º. Macor is a special type of glass-ceramic composed of fluorphlogopite mica and borosilicate glass. Its chemical composition includes about 46% silica (SiO_2), 17% magnesium oxide (MgO), 16% aluminum oxide Al_2O_3, 10% potassium oxide K_2O 7% boron trioxide B_2O_3, and 4% fluorine (F). The important property of Macor is its low thermal conductivity and capacity to withstand temperatures as high as 1000°C. The XRD unit lacked the specialised tools needed to examine the platinum thin films that had formed on the Macor substrate directly. Analysis of the Macor substrate itself is the first step towards overcoming this issue. To understand the Macor material's XRD pattern before the thin film deposition. Determining the characteristic peaks and diffraction angles associated with Macor was made possible by the first phase's establishment of a baseline. Continued using this baseline investigation to apply a layer of thin-film platinum on the Macor substrate. Following the film deposition, the following configurations were subjected to XRD experiments: By comparing the XRD patterns of these configurations, Macor alone and Macor with deposited Platinum film can be used to investigate any changes or shifts in the diffraction peaks. These changes might provide important new insights into the crystalline structure and orientation of the thin layers on the Macor substrate.

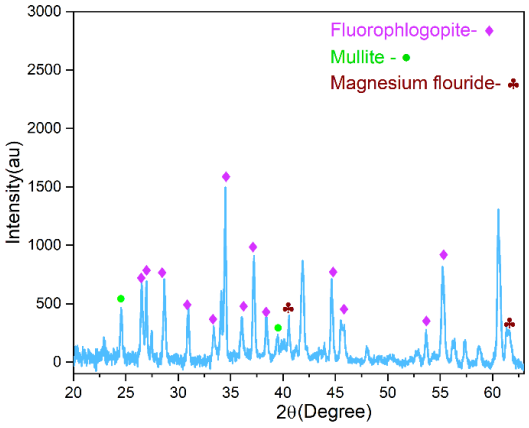

Fig.4: (a) XRD Pattern of Macor

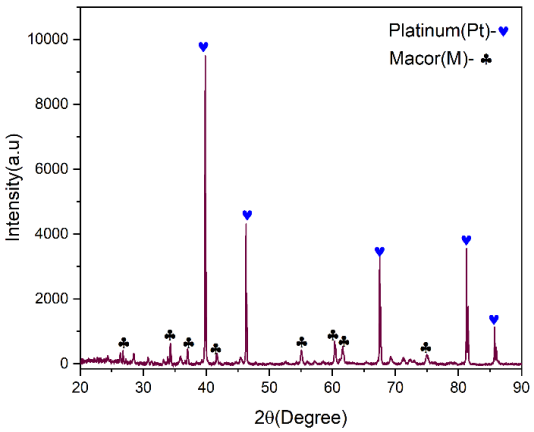

Fig.4: (b) XRD Pattern of Macor with Platinum thin film

Understanding the structural properties of the deposited platinum film and their possible uses in our research required completing this stage. As shown in Fig. 4(a). XRD pattern of Macor is presented, revealing its complex composition. Predominantly, Macor consists of fluorphlogopite as its major constituent. Moreover, our analysis identified the presence of two additional crystalline phases within Macor, namely Mullite and Magnesium Fluoride. As shown by the respective JCPDS (Joint Committee on Powder Diffraction Standards) card numbers for these three separate phases, the XRD profiles acquired from Macor show a substantial degree of conformity with reference patterns. The close match with the fluorphlogopite phase, characterized by JCPDS card number (16-0344), firmly establishes the significant presence of fluorphlogopite in the Macor material. Similarly, the significant level in line with the Mullite phase reference pattern, identified by the JCPDS card number (85-1460), confirms Mullite's presence as an important element of Macor. Furthermore indicating the existence of magnesium fluoride in the Macor composition is the tight alignment of the XRD pattern with the reference pattern for the magnesium fluoride phase, identified by the JCPDS card number (41-1443). This thorough validation not only confirms Macor's composition but also provides insightful information on the material's crystalline structure and the different stages that constitute it. The pattern of XRD is shown in Fig. 4(b). The Macor with a thin film of Platinum deposited onto its surface. This analysis reveals distinct peaks corresponding to the presence of the platinum film. Specifically, the platinum peaks are observed at angles of 39.27º, 45.66º, 66.56º, and 80.11º. These observed peaks closely align with the reference pattern of pure platinum, as documented in the JCPDS card number (84-2343). This agreement confirms the successful deposition of a platinum-thin film onto the Macor substrate. The additional peaks observed are attributed to the Macor. This confirms the existence of both Macor and Platinum thin film.

2.5. Optical Microstructure and Basic Morphology of Platinum TFG:

A (ZEISS Axio Lab A1 Microscope) which was equipped with a digital snapshot-capturing arrangement and a computerised monitoring system for precise inspection, was utilised for microstructural analysis. With the help of ImageJ software (version 1.50i), the obtained images were subjected to additional analysis, allowing for a thorough and systematic examination of the microstructure.

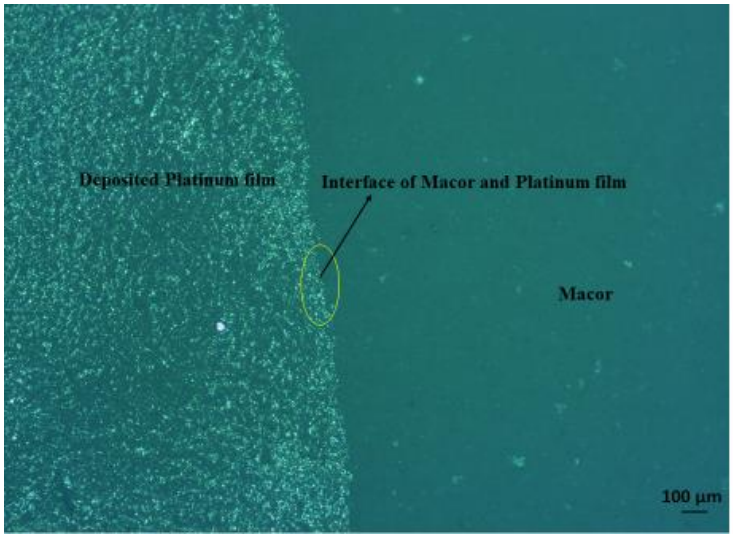

Fig.5: Interface region between Macor and deposited Platinum film

Fig.5. provides a thorough examination of the Macor and platinum microstructure, focusing on how it interacts with a tiny layer of platinum that has been formed. To enlarge the focus to the interface of the platinum film deposition on the Macor substrate. This region provides a closer look at any structural alterations or interactions occurring at the interface between these two materials, which could have an impact on the adhesion and integration of the film.

Then Microstructural analysis across the samples is investigated using a scanning electron microscope (SEM-JOEL 6380). The area fraction has been estimated using the ImageJ software (v1.50i) an average of 10 readings is taken for estimation with a scale of 20 µm.

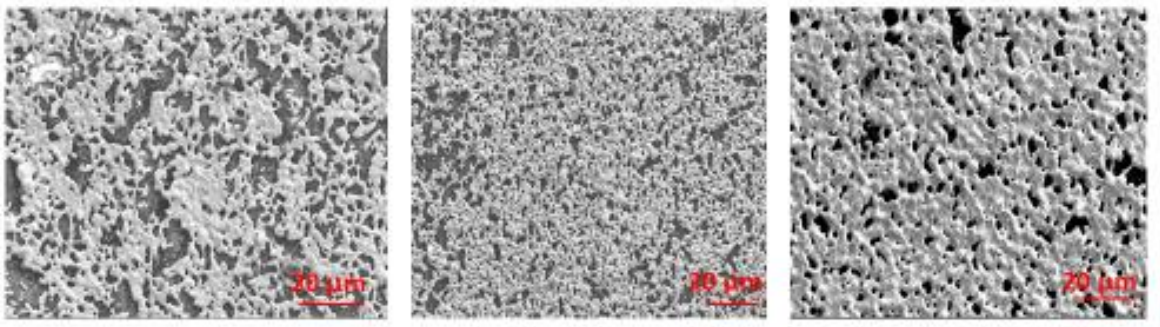

(a) 700°C (b) 800°C (c) 900°C

Fig.6: SEM image of the platinum Macor-based sensor at different temperatures.

Fig.6. shows the SEM images used to observe the deposited platinum morphology and interface region with the Macor substrate. The TFGs at three different temperatures 650 °C, 750 °C, and 900 °C have been used for SEM investigations. The white region in Fig.6. Represents the deposited platinum, and the remaining region represents the Macor substrate.

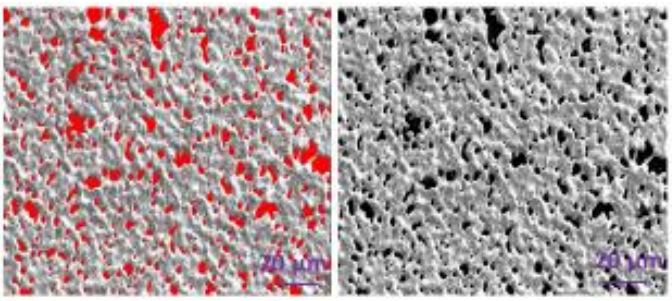

Fig.7: Area fraction of deposited platinum at 900℃

The area fraction of Platinum at 900 ℃ was calculated to be 88% as shown in Fig.7. With a scale of 20 µm. This implies that the platinum is distributed nearly uniformly throughout the substrate. The area fraction of platinum deposition at various temperatures is shown below.

Table 2: Area fraction values obtained after annealing heat treatment temperature.

Temperature (℃)	Area fraction (%)
700	64
800	70
900	88

This study aims to ascertain how the platinum is deposited after annealing. Higher annealing temperatures lead to an increase in the uniformity of film deposition and area fraction, as shown in Fig. 6. And Table 2.

3. TFG static calibration:

3.1 Set-up for an experiment

TCR and sensitivity are the two main criteria that define TFG performance. One method for assessing these characteristics is through static calibration, also referred to as oil bath calibration. Static calibration aids in analysing and assessing the linearity needed to estimate a TCR of TFGs. Fig. 8. Illustrates the experimental setup's schematic, built for this purpose. A pure silicone oil flask that is just partially filled and set up for static calibration on a heated plate. Another small empty beaker is fitted, so half of it should dip into silicone oil. Both the calibrated mercury glass thermometer and the TFGs are set at the same height inside the air flask, ensuring that they both measure the same temperature, the heater plate is powered on, and the silicone oil is heated. As silicone oil is known to be thermally and chemically stable at high temperatures, it serves as a heating agent for the air contained within the flask. A CCS is connected to a TFG, and then to the data acquisition system (DAS) (Model-Keithley 2450).

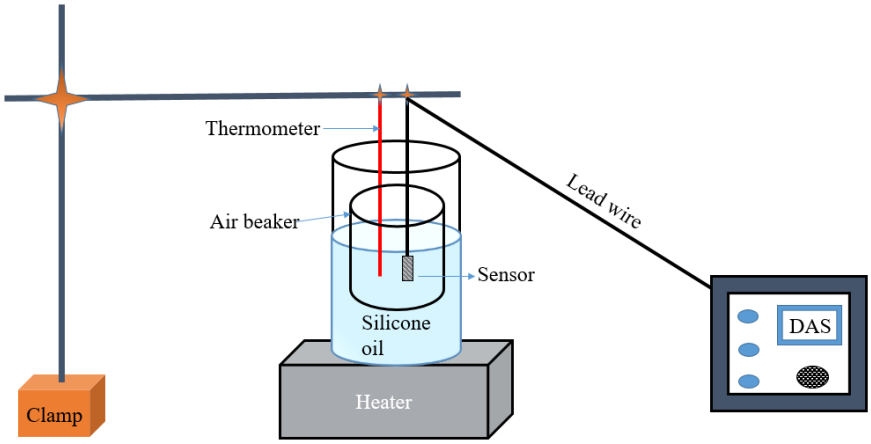

Fig.8: Sensor static calibration schematic

3.2 Sensitivity Measurement:

The temperature-sensitive film-based heat flux sensor is subjected to uniform heating and subsequently allowed to cool naturally during calibration in an oil bath technique to estimate the sensitivity. A CCS is used in these tests to provide TFGs with a steady current of 10 mA. After switching off the heater, the silicone oil bath is heated from 30 °C to 80 °C before cooling naturally. Accurately estimating TCR and sensitivity resistance and temperature measurements must be done with sufficient care. As indicated in Fig. 9. Resistance responses of TFG related to temperature are recorded in DAS during steady heating and natural cooling. A little resistance lag, and thermal hysteresis, have been seen between the heating and cooling operations. Here, it is observed that cooling resistance is lower than heating resistance at similar temperatures. The observed hysteresis is commonly linked to the contraction related to the thin film in the sensor due to the loss of thermal energy when it cools down [37]. This phenomenon applies to both sensors built in-house and commercially available ones. Based on the data obtained, a coefficient of correlation (r) of 0.99 was estimated for TFGs, indicating a linear relationship between resistance and temperature. This feature represents the application of TFGs in precise temperature measurements before predicting heat flux. Based on such resistance-temperature curves, sensitivity (S) is estimated.

This applies to the correlation between the variation in temperature and the corresponding alteration in resistance, which is expressed as an equation (Eq.1). The slope of the resistance versus temperature curve signifies the relationship between the two variables.

$$S=\frac{\Delta R}{\Delta T} \quad (1)$$

The table presents the most accurate linear regression equations used for calculating sensitivity. Here, R_h represents the resistance during heating, while R_c represents the resistance during cooling. Differentiating the linear fit equations gives sensitivity.

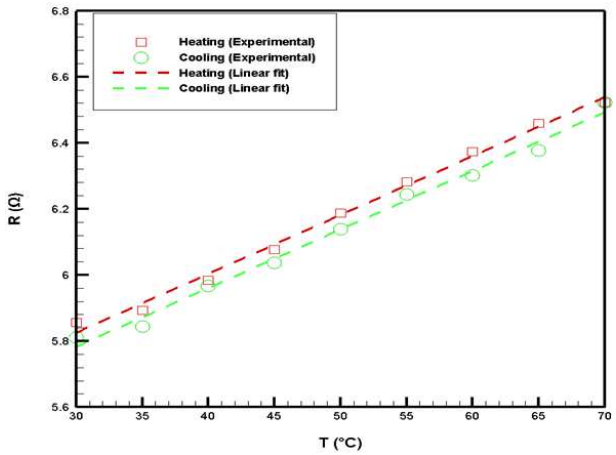

Fig.9: Sensor response to the static calibration

Table 3: Analysis of the sensor's sensitivity

Sensor	Best linear fit	Coefficient of correlation (r)	Average sensitivity (S) (ohm/K)
TFG	R_h =5.291 + 0.01782*T R_C=5.251 + 0.01773*T	0.994 0.991	0.017775

From the above table, the sensitivity for TFGs essentially corresponds to the linear relationship between resistance and roughness. Since that sensitivity is dependent on the resistance value of the TFGs enhanced sensitivity may also be attributed to the increase in electrical resistance [37]. An Ag-Carbon Nanotube (CNT) nanocomposite film was created as a sensing component for TFGs. The performance of the TFGs was then compared to pure Ag TFGs to evaluate their effectiveness [41]. It is recommended to use MWCNTs for measuring low heat flux and for substrates made of Macor because they require higher sensitivity to enhance the output response [42].

3.3 TCR Measurement:

The value of TCR dictates how well heat flow rates in steady state and during transient conditions are estimated. Because of this, Fig. 7 illustrates the resistance at a certain temperature compared to resistance at room temperature (R/R_0) across the temperature difference. To determine TCR, the first-order linear fit is used in these plots. Table 3 provides the appropriate first-order fit equations for different sensors for heating and cooling operations. The referenced standard equation is compared to this equation.

$$\frac{R}{R_0} = 1 + \gamma \Delta T \quad (2)$$

Here, R denotes the sensor's resistance response in any temperature range T,

at room temperature T_0 (30°C), the resistance is denoted by R_0, the temperature coefficient of resistance is represented by γ, and ΔT denotes the variation between a given temperature T and the ambient room temperature T_0.

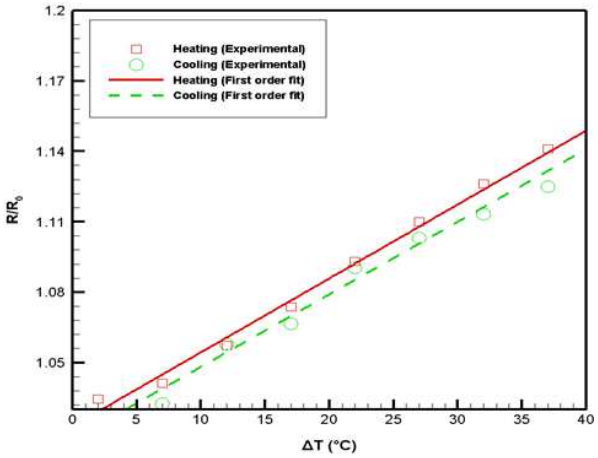

Fig.10: TCR estimation for the sensor

Table 4: Analysis of the sensor's TCR.

Sensor	First order fit	Average TCR (K^{-1})
TFG	$(R/R_0)_h$=1.023+ 0.003148*ΔT $(R/R_0)_c$=1.017+ 0.003091*ΔT	0.0031195

These findings demonstrate that TCR is roughness-dependent and that it increases as roughness increases. The main cause of this rise in TCR with roughness is an increase in resistance value [40].

4. TFGs Dynamic calibration:

Usually, convective-based studies include heat loads that are step- or impulse-like and last relatively short. The TFGs quick response time allows for the application of recording transient temperatures of short duration for convective heat loads that are uncertain [21]. A basic laboratory experiment has been built, and TFGs have been calibrated with given temperatures and velocities, along with their transient temperatures, to assess the similarity in step heating load. A one-dimensional heat conduction method has been utilised to calculate the heat flux at the surface. Based on a changing temperature over time. Furthermore, comparisons between the numerical simulation predictions and experimental situations have been examined.

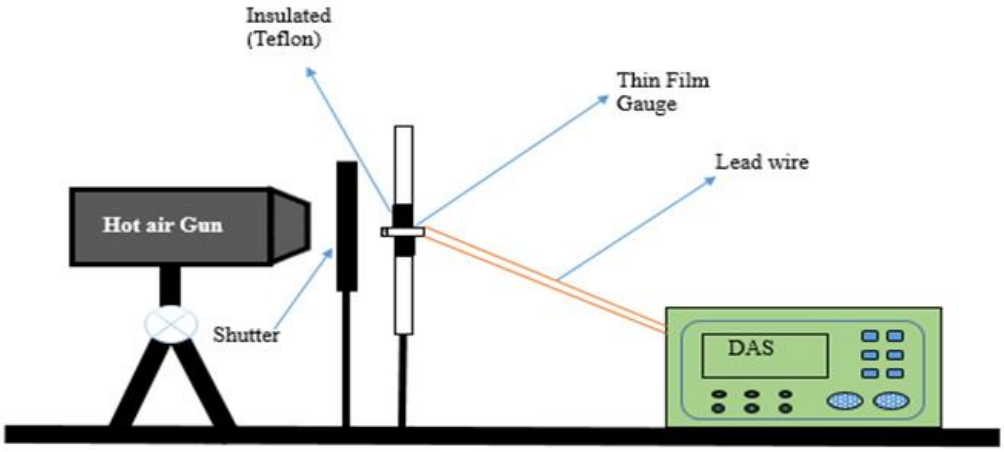

Fig.11: A schematic representation of a laboratory setup using a hot-air gun.

4.1 Experimental analysis using thin-film gauges:

The ultimate objective of convective-based calibration pertains to recording temperature responses, which is done by exposing the handmade thin film gauge to a heated environment. Fig.11. illustrates how a hot air gun provides heat to a thin film gauge for this intent. A heated air gun (Model number: HD3201) has an inbuilt heater that discharges hot air jets into an atmosphere with a range of operating points that have varying velocities and temperatures (6.60 m/s, 333 K) (11.50 m/s, 338 K) respectively. With a FLUKE 925 Vane anemometer, hot air velocity is recorded. As per the specified dimensions, it can produce up to 1,500 watts. The device consists of a gun head with a diameter of 30 mm, capable of generating a constant flow of hot air. The homemade thin film gauge has its axis matched with the axis of the hot air gun and is fixed 20 mm from the exit nozzle (Fig. 11). The thin film gauge and hot air gun nozzle are separated by a shutter, which is kept closed until the flow from the gun is fully developed. After the hot air gun has reached a fully developed flow pattern, the shutter has been removed. To enable the hot air from the gun jet to pass over the thin film gauge. The thin film gauge convective heating experiment is performed using the same experimental setting, and DAS is used to record the sensor's response. The temperature-time histories are generated from these voltage or resistance signals, and DAS is used for recording transient temperature profiles. Fluctuating heat flux is produced by the hot air flow from the hot air gun, which is not homogeneous.

The experiment's consistency has been examined. By experimenting multiple times with the Macor-based platinum sensor, the thin film's sensitivity and the substrate's properties independently determine how a sensor responds to changes in temperature. Irrespective of its sensitivity, a Macor-based sensor responds to heat flux with a higher temperature. The recorded standard resistance signals from the PTFG after performing several iterations of the experiment. It is clear that the gauge reacts instantly to the hot-air jet that is passing by, and the following time constants are given for the two operating modes: For the first case, the thermal time constant, as obtained from the mean temperature plot in Fig. 13 (b), is approximately 0.426 seconds, and for the second case, the thermal time constant, also derived from the mean temperature plot in Fig. 14 (d), is approximately 0.87 seconds. The average thermal time constant for PTFG is calculated to be 0.648 seconds by using the mean temperature plot. It is calculated experimentally as the time it takes the system to achieve 63.2% of the full-scale average [44]. The observation can be attributed to the inverse correlation between the temperature response and thermal effusivity of the substrate. This inverse relationship can be expressed as $\sqrt{\rho_s C_s k_s}$ in $\rho_s, C_s \; and \; k_s$ refers to the density, specific heat, and thermal conductivity of the substrate material, respectively. This statement can be reinforced by referring to Equation 3, which describes the temperature change caused by a specific heat transfer in a semi-infinite solid [42].

$$(T\text{-}T_0) = \frac{2q\sqrt{\frac{t}{\pi}}}{\sqrt{\rho_s C_s k_s}} e^{\left(\frac{x^2}{4\alpha_s t}\right)} - \frac{qx}{k}\left[1 - \operatorname{erf}\left(\frac{x}{2\sqrt{\alpha_s t}}\right)\right] \quad (3)$$

Here q represents a constant heat flux in (kW/m^2), α_s $(=\frac{k_s}{\rho_s C_s})$ is the substrate's thermal diffusivity in (m^2/s), the variable t represents the duration of the test in seconds, while x represents the distance from the substrate surface in meters. The substrate thermal effusivity, $\sqrt{\rho_s C_s k_s}$ in ($J/m^2s^{0.5}$ K) is also a significant factor. When measuring the temperature changes caused by a heat flux applied to the surface at a single location, x can be set to 0 in Equation 4. Hence Eq.3 has been reduced to

$$T = \frac{2q\sqrt{\frac{t}{\pi}}}{\sqrt{\rho_S C_S k_S}} + T_0 \quad (4)$$

The substrate thermal effusivity is inversely associated with the surface temperature of a sensor, based on the stated equation. Therefore, in current studies, there is a preference for utilizing the substrate material as a Macor in producing thin film sensors. Amplification is suggested as it can improve temperature signalling for certain heat loads. This augmentation can be particularly important when measuring lower heat flux values.

4.2 Numerical analysis using PTFGs:

The continuous advancements in computer technology have made it possible to utilize numerically based physical simulation concepts in various sciences as well as engineering fields [43]. This research aims to provide information on parameters and assess heat flow using the current experimental parameters at the sensor region. Convective heat load is numerically analysed for a range of input values for velocity and temperature which are (6.60 m/s, 333 K) and (11.50 m/s, 338 K), and as atmospheric outlet constant pressure (1.01325 bar) and temperature of 300 K throughout all walls has been applied and simulated by platinum-based thin film gauge utilizing commercial ANSYS-FLUENT software. The primary focus of this simulation is to give us an understanding of flow facilities as well as assess heat flux under the most common test conditions. A numerical simulation of the two-dimensional model was created using the ANSYS workbench.

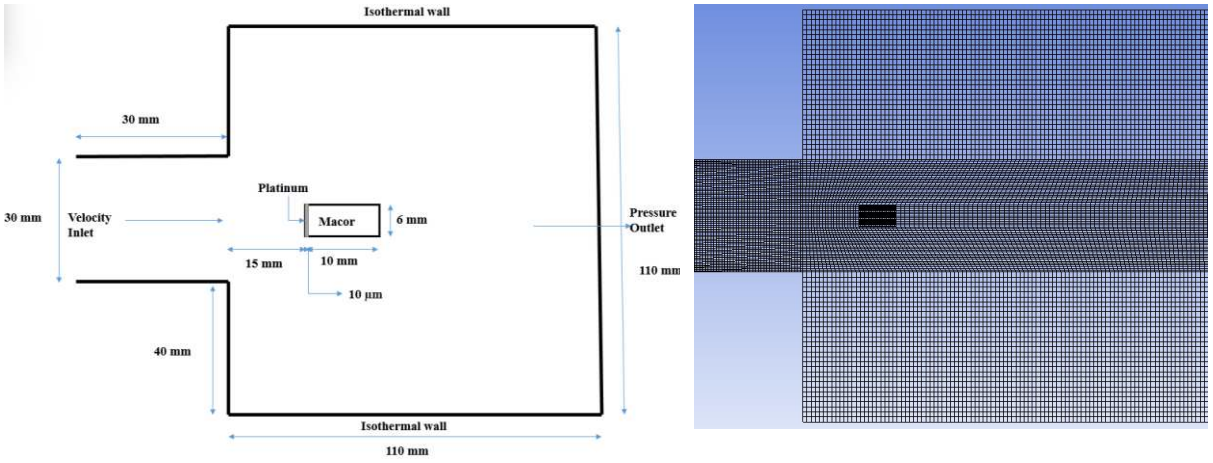

(a) (b)

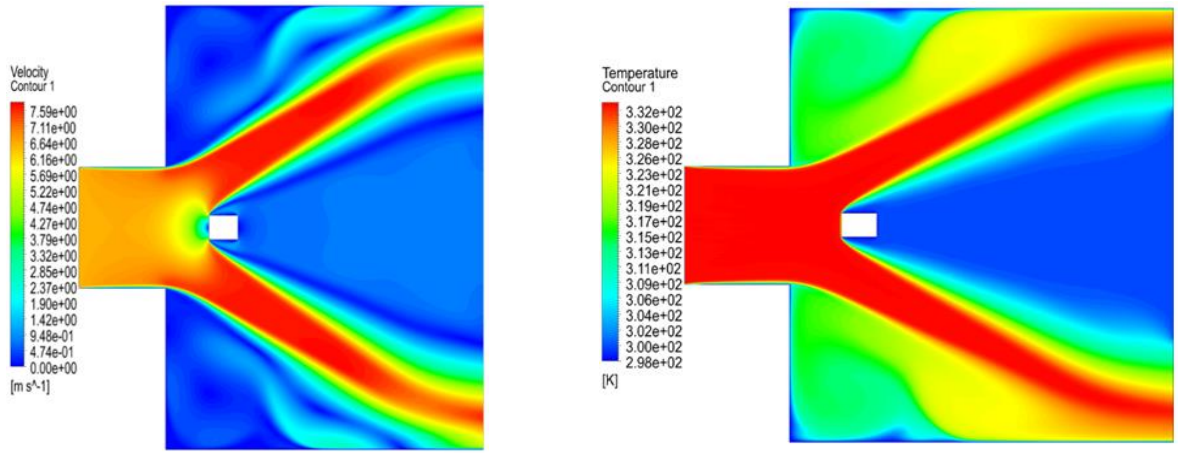

(c) (d)

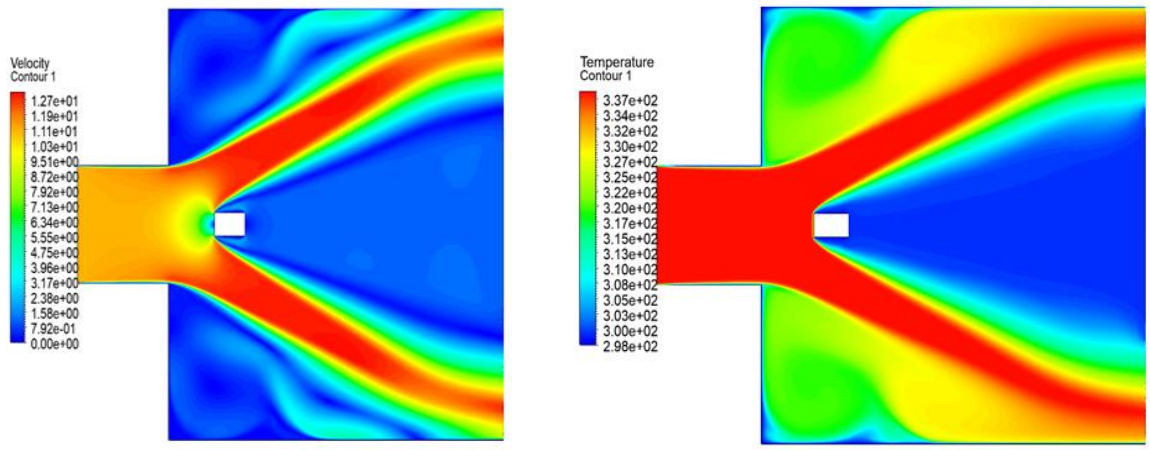

(e) (f)

Fig.12: (a) An analysis model; (b) Mesh model; (c, e) Velocity distribution contour; (d, f) Temperature distribution contour.

The platinum coating thickness is 10 µm in the sensor model created by ANSYS. The supporting material Macor, a 6 mm diameter, and a 10 mm length are offered. The mesh creation for such a dimension has been an important parameter because the platinum portion of the modelling is too thin. A two-dimensional geometry model is created using the Ansys workbench. A structured grid was created for the finite volume method, and the mesh size was optimized through a grid-independent study to minimize errors. A thorough mesh refinement process within the platinum thin film and its adjacent regions to capture temperature gradients. Thus the grid element sizes of 0.001 mm along the x-axis and 0.06 mm along the y-axis, while maintaining a mesh size of 0.759 mm in the other fluid domain have been employed. Grid sensitivity investigations were carried out using 75000, 160,000, and 250,000 cells. According to the study, the existing results using 250,000 cells are almost invariant to further grid refinement. Fig.12 (a-b) illustrates the fluid zone and mesh structure.

Numerical analysis is carried out on experimental parameters by supplying heated air into the flow field through a 30 mm diameter and conducting the flow only in an axial direction. The impact of vertical flow has not been considered at the inlet. The PTFG made of Macor was positioned 15 mm away from the inlet, as this location was predicted to have the highest velocity. The flow occurred horizontally, and computation was performed on a 110 mm horizontal and 110 mm vertical length domain. The time step size has just been set at 1 ms for 100 steps of that number. The number of iterations that can be performed is set at 40, and the convergence criterion set is 10^{-6} With a no-slip boundary condition, the walls are treated as Isothermal. A computational domain's exit is part of the pressure outlet. The contour demonstrates the total temperature and velocity profiles across its flow direction. The velocity contour in the direction of flow is shown in Fig.12 (c, e). At the tip of the macro-based PTFG, the velocity is zero due to the abrupt cessation of fluid flow by a body, which leads to zero velocity at the contact region. In Fig.12. (d, f), the maximum temperature is registered by a total temperature contour for the flow direction at the tip of the PTFG. The entire kinetic energy has transformed into thermal energy. At the tip, the velocity is zero, resulting in the highest temperature.

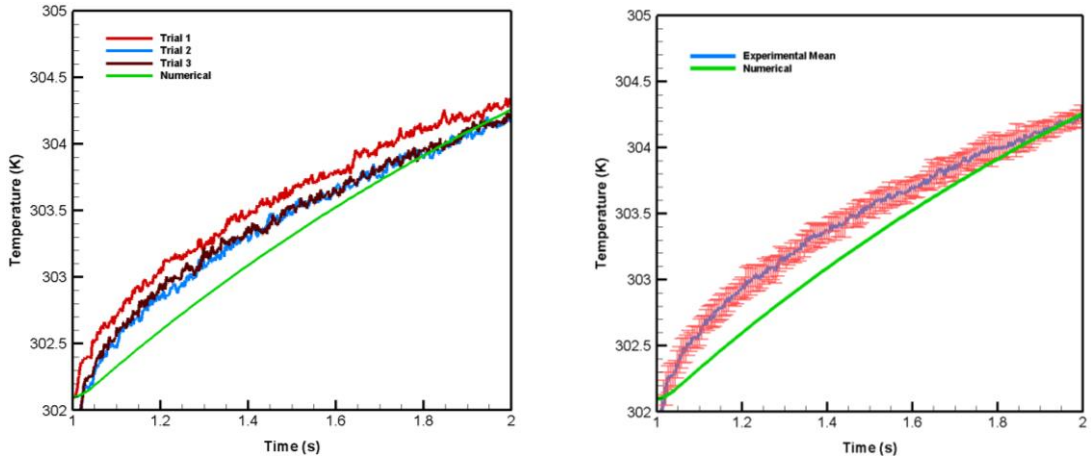

(a) (b)

Fig.13: Temperature response of the sensor for a given number of trials using the heat gun's first setting (6.60 m/s, 333 K).

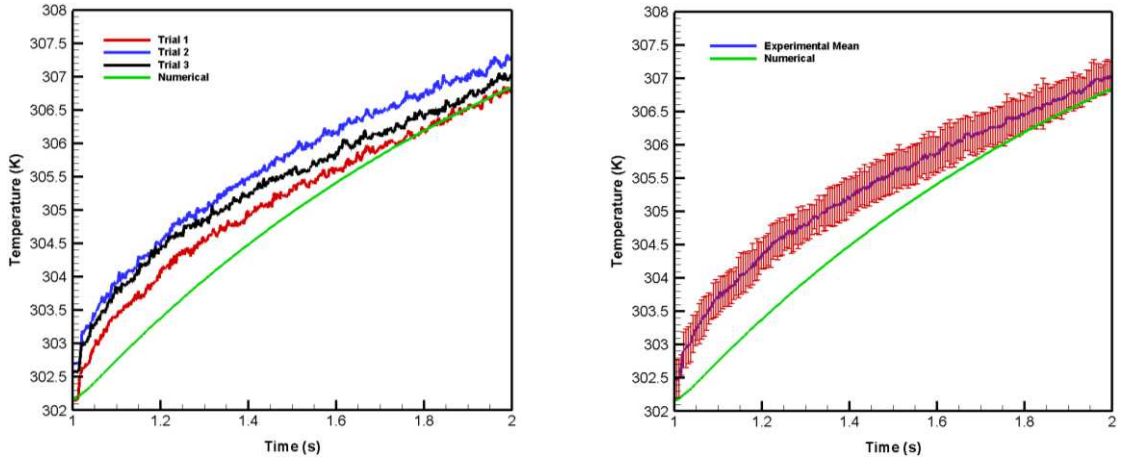

(c) (d)

Fig.14: Temperature response of the sensor for a given number of trials using the heat gun's second setting (11.50 m/s, 338 K).

Fig.12. (c–f) illustrates the contour at 6.60 m/s velocity and a temperature of 333 K. When the inlet air velocity and temperature are both 11.50 m/s and 338 K, the behavior of these contours remains the same. A finite volume approach using ANSYS-FLUENT and the mentioned boundary conditions is used to estimate how well the PTFG will perform in low-speed flow. Fig. 13(a)–14(d) represents the transient temperature variation as a function of time in which Fig. 13 (a–b) depicts variations for a velocity of 6.60 m/s, temperature of 333 K, and Fig.14 (c-d) are shown for a velocity of 11.50 m/s, temperature of 338 K respectively, numerically and experimentally. Fig. 13 (a) and 14 (c) represent the experimental temperature response for 3 trials along with numerical analysis. Similarly, Fig. 13 (b) and 14 (d) represent the experimental mean temperature of three trials, with error bars showing the uncertainty. The red error bars in Fig. 13 (b) and 14 (d) indicate the average standard deviation of these measurements, which are (±7.94% and ±27%), respectively. The associated and essential relative difference among mean experimental and numerical parabolic temperature variations with time variations is 0.14% for PTFG, respectively, when the temperature is 333 K, and the input velocity is 6.60 m/s while applying 338 K temperature and 11.50 m/s velocity. The mean experimental and numerical variations in percentage is 0.33% for PTFG, respectively. Heat loss throughout the experiment causes a variation in temperature change between the

experimental and numerical measurements. Temperature mean values that do not deviate by more than 0.5% are considered satisfactory and sufficient.

5. Estimating surface heat flux:

When assessing heat conduction in a semi-infinite solid using a one-dimensional approach, it is possible to predict heat flux by analyzing the surface temperature history. The assumptions in this recovery are as follows. i) The sensing element's temperature measurement reflects the substrate surface temperature due to the film's thinness. ii) Heat transfer is restricted to the axial direction (perpendicular to the surface) without transverse heat conduction. iii) The thermal behavior of substrate materials remains constant. iv) Since the substrate is infinitely long, there is no temperature rise at either end of the substrate during short test periods. These assumptions result in a solution that is expressed as [37].

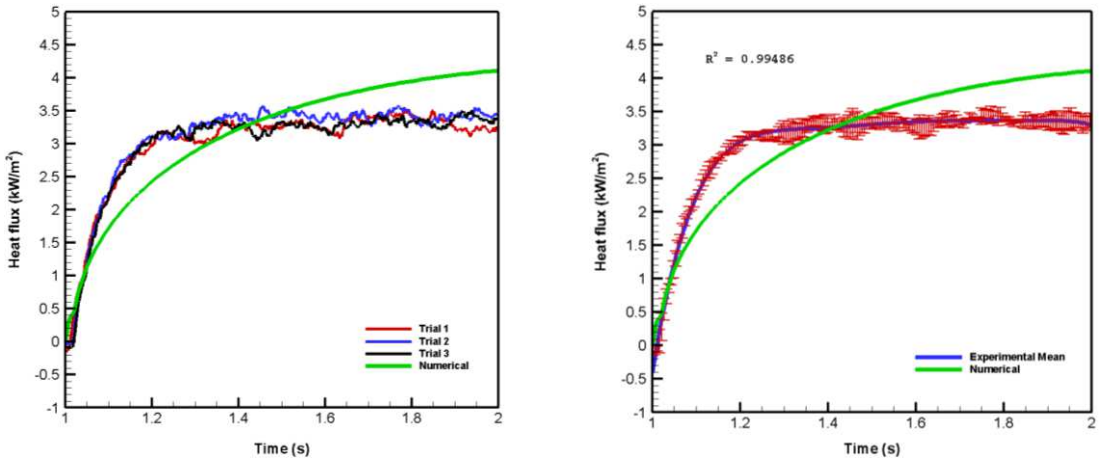

(a) (b)

Fig.15: Heat flux response of the sensor for a given number of trials using the first setting of a heat gun (6.60 m/s, 333 K).

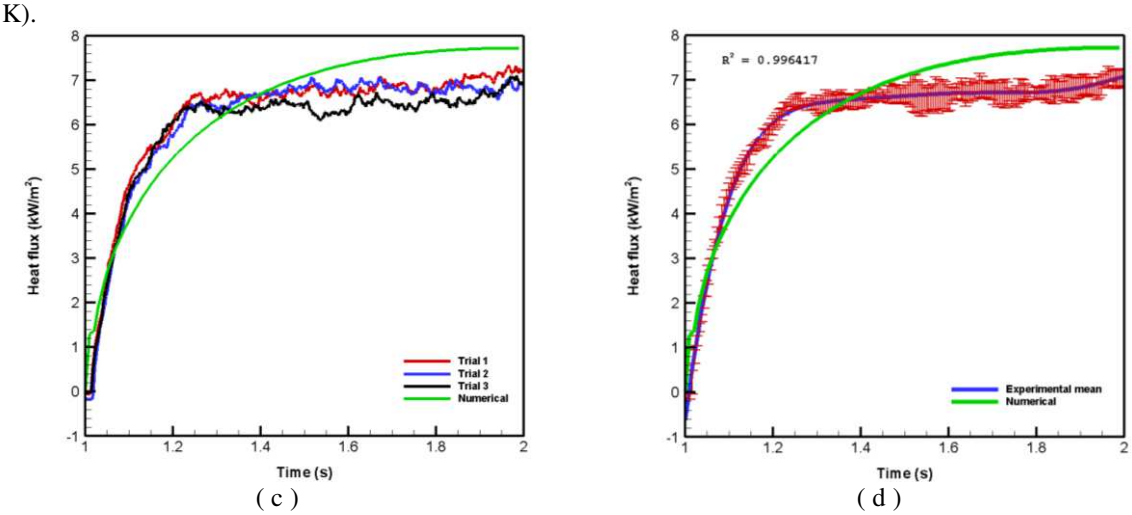

(c) (d)

Fig.16: The heat flux response of the sensor was recorded during several trials using the second setting of the heat gun (11.50 m/s and 338 K).

Table 5: for the thin film gauge heat transfer, Surface heat flux is determined using temperature histories.

Sensor	Load 1 Average Heat flux (kW/m^2) Experimental/Numerical	Load 2 Average Heat flux (kW/m^2) Experimental/Numerical
TFGs	2.997/3.131	6.204/6.347
	3.095/3.131	6.111/6.347
	3.001/3.131	5.933/6.347

$$q(t)=\frac{\sqrt{\rho_s C_s k_s}}{\pi}\int_0^t \frac{1}{\sqrt{t-\tau}}\frac{d\{T_s(\tau)\}}{d\tau}d\tau \quad (5)$$

In this equation, q (t) represents the heat flux that varies with time, while ρ_s, c_s, and k_s refer to the substrate material's density, specific heat, and thermal conductivity, respectively. $T_s(\tau)$ is the substrate surface temperature. The temperature signal must be discretized to solve the above equation numerically. Researchers have examined a variety of discretization techniques. The cubic spline technique is the discretization method that is most frequently utilized. References provide more details on this technique [36-40].

The calculated heat flux derived from the heat transfer gauge transient temperature history is shown in Fig. 15 (a)–16 (d) for different flow conditions. Fig. 15 (a–b) illustrates the variation for a 6.60 m/s speed and a 333 K temperature. Fig. 16 (c-d) for 11.50 m/s and 338K. Fig. 15 (a) and 16 (c) represent the experimental heat flux response for 3 trials along with numerical analysis. Similarly, Fig. 15 (b) (For Experimental with R^2 =0.9948 and Numerical with R^2 = 0.9904) and 16 (d) (For Experimental with R^2 =0.9964 and for Numerical with R^2 = 0.984) represent the mean heat flux of three trials, with error bars showing the uncertainty. The red error bars in Fig. 15 (b) and 16 (d) indicate the average standard deviation of these measurements, which are (±9% and ±19.38%), respectively. The associated and essential relative difference among average experimental and numerical heat flux variations with time variations is 3.3% for PTFG, respectively, when the temperature is 333 K and the input velocity is 6.60 m/s while applying 338 K temperature and 11.50 m/s velocity. The average experimental and numerical variations in percentage are 4.17% for PTFG, respectively. The one-dimensional heat conduction model in Eq. (5) is used to estimate the heat fluxes in a semi-infinite model. The data are analysed and closely compared, and it was observed that there is good agreement with minimal deviation. It is found that these hand-made PTFGs can detect at low temperature and low-velocity conditions after being manufactured and calibrated with two types of flow situations. The experimental findings closely align with the numerical results.

Uncertainty Analysis:

The measurement uncertainty is discussed in this section**.** The substrate roughness measurement uncertainty in the current work is ±0.26 %**.** Resistance measurement inaccuracy in static calibration is ±0.012%, hot air gun's uncertainty value is ±0.03% while temperature measurement uncertainty is ± 0.96%. The heat flux delivered has a ±1.8% uncertainty during dynamic calibration. In TCR estimation, there is ±0.29% uncertainty. Uncertainties in the material properties of the substrate can be used to evaluate the uncertainty of heat flux prediction. For density, specific heat, and thermal conductivity, respectively, the uncertainties in Macor thermophysical properties are now measured at ±0.5%, ±2%, and ±3% [39]. Based on these data, the range of the uncertainties investigated for short-term temperature signals is between ±0.25% and ±0.35%, and for heat flux signals between ±0.40% and ±0.50%. These uncertainties are all within an acceptable ±2% range.

6. Conclusion:

This study revealed that increasing the annealing heat treatment temperature results in improved adhesion of thin films. Additionally, an increase in the resistance of TFG leads to enhanced sensitivity. This demonstrates the valuable applicability of TFG in challenging environments, particularly in the context of hypersonic harsh conditions, where strong film adhesion is important. Present research findings support the utility of these TFGs for both high and low heat flux measurements, thus establishing their relevance across a range of applications like air monitoring in smokestacks, cooling towers within coal plants, combustion of air in boilers, HVAC duct fires, smoke detectors, etc.

The key research performance outcomes have been quantified and are presented below.

- The TCR was determined to be 0.0031195 K^{-1}, and the sensitivity was found to be 0.017775 ohm/K.
- Based on the mean temperature plot, the average thermal time constant for TFG is estimated to be 0.648 seconds.
- The average heat flux for various input velocities stepped out to be 3.031 kW/m^2 and 6.0826 kW/m^2, respectively, and the measurements' respective average standard deviations are (±9% and ±19.38%).
- To assess temperature time variation and heat flow, numerical analysis using FLUENT has been done based on experimental conditions. For three separate shots, the procedure is carried out numerically and experimentally with an acceptable error difference in the range of ± 5%.

Acknowledgments:

The authors would like to acknowledge the Department of Science and Technology- Science and Engineering Research Board (DST-SERB) for their financial support in the development of thin film gauges and provision of essential experimental facilities under Project Number- ECR/2017/000260.

References:

[1] Holmberg, D., Steckler, K., Womeldorf, C., & Grosshandler, W. (1997, November). Facility for calibrating heat flux sensors in a convective environment. In ASME International Mechanical Engineering Congress and Exposition (Vol. 18428, pp. 165-171). American Society of Mechanical Engineers. https://doi.org/10.1115/IMECE1997-0906

[2] Jones TV, Oldfield MLG, Ainsworth RW, Arts T (1993) Transient cascade testing, NATO advanced Group for Aerospace Research and Development AG328 (Chapter 5).

[3] Marom, H., & Eizenberg, M. (2006). The effect of surface roughness on the resistivity increase in nanometric dimensions. *Journal of applied physics*, *99*(12). https://doi.org/10.1063/1.2204349

[4] Vidal RJ (1956) Model instrumentation techniques for heat transfer and force measurements in a hypersonic shock tunnel. Cornell Aeronautical Laboratory, Report No WADC TN 56-315.

[5] Kaser A, Gerlach E (1995) Scattering of conduction electrons by surface roughness in thin metal films. Zeitschrift für Physik B Condensed Matter 97(1):139–146. https://doi.org/10.1007/BF01317598

[6] Buttsworth DR, Jones TV (1998) a fast-response total temperature probe for unsteady compressible flows. J Eng Gas Turbines Power 120(4):694–702. https://doi.org/10.1115/1.2818456

[7] Palasantzas, G., & Barnaś, J. (1997). Surface-roughness fractality effects in electrical conductivity of single metallic and semiconducting films. *Physical review B*, *56*(12), 7726. https://doi.org/10.1103/PhysRevB.56.7726

[8] Krzak-Ros J, Filipiak J, Pezowicz C, Baszczuk A, Miller M, KowalskiM, Bedzinski R (2009) The effect of substrate roughness on the surface structure of TiO2, SiO2, and doped thin films prepared by the sol-gel method. Acta of Bioengineering and Biomechanics 11(2):21–29.

[9] Peng, Z. L., & Chen, S. H. (2011). Effects of surface roughness and film thickness on the adhesion of a bioinspired nanofilm. *Physical Review E*, *83*(5), 051915. https://doi.org/10.1103/PhysRevE.83.051915

[10] Miller CG III (1981) Comparison of thin-film resistance heat transfer gauges with thin skin transient calorimeter gages in conventional hypersonic wind tunnels. NASA Technical Memorandum, 83197.

[11] Persson, B. N., & Scaraggi, M. (2014). Theory of adhesion: Role of surface roughness. *The Journal of Chemical Physics*, *141*(12). https://doi.org/10.1063/1.4895789

[12] Ainsworth RW, Schultz DL, Davies MRD, Forth CJP, Hildith MA, Oldfield MLG, Sheard AG (1988) Developments in instrumentation and processing for transient heat transfer measurement in full stage model turbine. ASME 88-GT-11. https://doi.org/10.1115/1.3262232

[13] Iliopoulou V, Denos R, Billiard N, Arts T (2004) Time-averaged and time-resolved heat flux measurements on a turbine stator blade using two-layered thin-film gauges. In ASME Turbo expo 2004: power for land, sea, and air (pp. 553–561). https://doi.org/10.1115/1.1791647

[14] Prajapati, H., & Deshmukh, N. N. (2019). Design and development of thin wire sensor for transient temperature measurement. *Measurement*, *140*, 582-589. https://doi.org/10.1016/j.measurement.2019.04.020

[15] Epstein AH, Guenette GR, Norton RJG, Yuzhang C (1985) High-frequency response heat flux gauge for metal blading. In AGARD heat transfer and cooling in gas turbines 16 p (SEE N86-29823 21-07).

[16] Sahoo N, Saravanan S, Jagadeesh G, Reddy KPJ (2006) Simultaneous measurement of aerodynamic and heat transfer data for large angle blunt cones in a hypersonic shock tunnel. Sadhana 31(5):557–581 https://doi.org/10.1007/BF02715914

[17] Taler, J. (1996). A semi-numerical method for solving inverse heat conduction problems. *Heat and mass transfer*, *31*(3), 105-111. https://doi.org/10.1007/BF02333307

[18] Zubair SM (1993) Heat conduction in a semi-infinite solid subject to time-dependent surface heat fluxes: an analytical study. Heat Mass Transfer 28(6):357–364. https://doi.org/10.1007/BF01539534

[19] Kumar, R., Sahoo, N., Kulkarni, V., & Singh, A. (2011). Laser based calibration technique of thin film gauges for short duration transient measurements. *J. Thermal Sci. Eng. Appl.* Dec 2011, 3(4): 044504. https://doi.org/10.1115/1.4005075

[20] Kumar, R., Sahoo, N., & Kulkarni, V. (2012). Conduction based calibration of handmade platinum thin film heat transfer gauges for transient measurements. *International journal of heat and mass transfer*, *55*(9-10), 2707-2713. https://doi.org/10.1016/j.ijheatmasstransfer.2012.01.026

[21] Desikan, S. L. N., Suresh, K., Srinivasan, K., & Raveendran, P. G. (2016). Fast response co-axial thermocouple for short duration impulse facilities. *Applied Thermal Engineering*, *96*, 48-56. https://doi.org/10.1016/j.applthermaleng.2015.11.074

[22] Kumar, R., Sahoo, N., & Kulkarni, V. (2010, January). Design, fabrication and calibration of heat transfer gauges for transient measurement. In *ASME International Mechanical Engineering Congress and Exposition* (Vol. 44496, pp. 17-23). https://doi.org/10.1115/IMECE2010-40253

[23] Sahoo N, Kumar R (2016) Performance assessment of thermal sensors during short-duration convective surface heating measurements. *Heat and Mass Transfer* 52(9):2005–2013. https://doi.org/10.1007/s00231-015-1694-0

[24] Kumar, R., & Sahoo, N. (2013). Dynamic calibration of coaxial thermocouples for short-duration transient measurements. *Journal of heat transfer*, *135*(12), 124502. https://doi.org/10.1115/1.4024593

[25] Jadhav, A., Kulkarni, V., & Peetala, R. K. (2020). Influence of substrate roughness on calibration parameters and thermal performance of thin film gauge. *Heat and Mass Transfer*, *56*, 2569-2583. https://doi.org/10.1007/s00231-020-02887-w

[26] Rout, A. K., Sahoo, N., & Kalita, P. (2021). Transient Response Characteristics and Performance Assessment of a Calorimetric Surface Junction Probe under Impulsive Thermal Loading. *Journal of Heat Transfer*, *143*(6), 062901. https://doi.org/10.1115/1.4050822

[27] Goswami, R., & Kumar, R. (2019). Dynamic calibration of temperature sensors from light rays for transient measurement. *Thermal Science*, *23*(3 Part B), 1901-1910. https://doi.org/10.2298/TSCI170303198G

[28] Nguyen, T. P., Thiery, L., Euphrasie, S., Lemaire, E., Khan, S., Briand, D., & Vairac, P. (2019). Calibration tools for scanning thermal microscopy probes used in temperature measurement mode. *Journal of Heat Transfer*, *141*(7), 071601. https://doi.org/10.1115/1.4043381

[29] Sarma S, Sahoo N, Unal A (2016) Calibration of a silver thin film gauge for short duration convective step heat load. Sadhana 41(7): 787–794. https://doi.org/10.1364/OE.23.007237

[30] Tiggelaar, R. M., Sanders, R. G., Groenland, A. W., & Gardeniers, J. G. (2009). Stability of thin platinum films implemented in high-temperature microdevices. *Sensors and Actuators A: Physical*, *152*(1), 39-47. https://doi.org/10.1016/j.sna.2009.03.017

[31] Hamdi, M., & Ektessabi, A. M. (2001). Influence of annealing temperature on simultaneous vapor deposited calcium phosphate thin films. *Journal of Vacuum Science & Technology A: Vacuum, Surfaces, and Films*, *19*(4), 1566-1570. https://doi.org/10.1116/1.1380228

[32] Cho, S., & Joshi, Y. (2019). Thermal performance of microelectronic substrates with submillimeter integrated vapor chamber. *Journal of Heat Transfer*, *141*(5), 051401. https://doi.org/10.1115/1.4042328

[33] Alam, T., & Kumar, R. (2021). Evaluation of response characteristics of thin film gauge for conductive heat transfer mode. *Transactions of the Institute of Measurement and Control*, *43*(3), 687-699. https://doi.org/10.1177/0142331220960665

[34] Cook WJ, Felderman EJ (1966) Reduction of data from thin-film heat-transfer gages-a concise numerical technique. AIAA J 4(3): 561–562. https://doi.org/10.2514/3.3486

[35] Zhuang, J. R., Werner, K., & Schlünder, E. U. (1995). Study of the analytical solution to the heat transfer problem and surface temperature in a semi-infinite body with a constant heat flux at the surface and an initial temperature distribution. *Heat and Mass Transfer*, *30*(3), 183-186. https://doi.org/10.1007/BF01476528

[36] Sahoo N, Peetala RK (2011) Transient surface heating rates from a nickel film sensor using inverse analysis. Int J Heat Mass Transf 54(5–6):1297–1302. https://doi.org/10.1016/j.ijheatmasstransfer.2010.11.029

[37] Žužek V, Batagelj V, Bojkovski J (2010) Determination of PRT hysteresis in the temperature range from−50 °C to 300 °C. Int J Thermophys 31(8–9):1771–1778. https://doi.org/10.1007/s10765-010-0823-8

[38] Sahoo, N., & Peetala, R. K. (2010). Transient temperature data analysis for a supersonic flight test. https://doi.org/10.1115/1.4001128

[39] Collins M, Chana K, Povey T (2015) new technique for the fabrication of miniature thin film heat flux gauges. Meas Sci Technol 26(2):025303. http://doi.org/10.1088/0957-0233/26/2/025303

[40] Kinnear, K., & Lu, F. (1997). Design, calibration and testing of transient thin film heat transfer gauges. In *20th AIAA advanced measurement and ground testing technology conference* (p. 2504). https://doi.org/10.2514/6.1998-2504

[41] Sarma, S., Singh, S., & Garg, A. (2021). Laminated Ag and Ag/CNT nanocomposite films as sensing elements for efficient thin-film temperature sensors. *Measurement*, *172*, 108876. https://doi.org/10.1016/j.measurement.2020.108876

[42] Jadhav, A., Peetala, R., & Kulkarni, V. (2020). Multi-walled carbon nano-tubes for performance enhancement of thin film heat flux sensors. *Heat and mass transfer*, *56*, 1537-1549. https://doi.org/10.1007/s00231-019-02765-0

[43] Manjhi, Sanjeev Kumar, and Rakesh Kumar. "Transient heat flux measurement analysis from coaxial thermocouples at convective based step heat load." *Numerical Heat Transfer, Part A: Applications* 75, no. 3 (2019): 200-216. https://doi.org/10.1080/10407782.2019.1580955

[44] Doebelin E O 1990 Measurement systems application and design. 4th ed., McGraw-Hill Publishing Company, Singapore.